Chapter 9
GaN Nanowall Network: Laser Assisted Molecular Beam Epitaxy Growth and Properties

M. Senthil Kumar and Sunil S. Kushvaha

9.1 Introduction

Group III-nitride materials, such as InN, GaN, AlN and their alloys, are the well-established semiconductors for the fabrication of high efficiency blue/green light emitting diodes (LEDs) and laser diodes (LDs) [1–3]. III-nitride LEDs are also the backbone for the current solid state lighting technology [4, 5]. Because of small size, light weight, high efficiency and long life time, nitride LEDs find a wide range of applications in the field of room lighting, displays, traffic lights, automobiles, etc. The excellent physical properties of group III-nitrides such as direct bandgap with a large tunability, high carrier mobility, high electron saturation velocity, high breakdown field, good mechanical and thermal conductivity, radiation hardness etc. are behind this success and make III-nitrides second most important semiconductors after silicon. Some of the important properties of wurtzite III-nitride semiconductors are listed in Table 9.1 [6–8]. Currently, III-nitrides are being explored for their potential applications in the field of short wavelength optoelectronics, high power electronics, photovoltaics and spintronics as well. Efficient AlGaN based ultraviolet (UV) LEDs are soon expected to replace UV lamps as they are free from ozone generation and mercury. On the other hand, the in-built spontaneous and piezo-electric polarization fields of GaN have led the way to realize AlGaN/GaN heterostructure based high electron mobility transistors (HEMTs) for micro- and millimeter-wave power electronics [9, 10]. Due to their robust nature, GaN based HEMTs can be used in extreme environmental applications such as space, satellite, and military systems.

M. Senthil Kumar (✉) · S.S. Kushvaha (✉)
CSIR-National Physical Laboratory, Dr. K.S. Krishnan Road,
New Delhi 110012, India
e-mail: senthilmk@nplindia.org

S.S. Kushvaha
e-mail: kushvahas@nplindia.org

© Springer Nature Singapore Pte Ltd. 2017

Z.H. Khan (ed.), *Recent Trends in Nanomaterials*,
Advanced Structured Materials 83, DOI 10.1007/978-981-10-3842-6_9

Table 9.1 Important physical properties of wurtzite III-nitride semiconductors [6–8]

Property		InN	GaN	AlN
Lattice constants	a (Å)	3.533	3.189	3.112
	c (Å)	5.693	5.185	4.982
Band gap energy E_g (eV) at 300 K		0.64	3.43	6.14
Exciton binding energy (meV)		9	34	60
Thermal expansion	$\Delta a/a$ (K^{-1})	3.8×10^{-6}	5.6×10^{-6}	4.2×10^{-6}
	$\Delta c/c$ (K^{-1})	2.9×10^{-6}	3.2×10^{-6}	5.3×10^{-6}
Thermal conductivity (W cm^{-1} K^{-1})		~0.8	1.3	2.85
Dielectric constant (ε_r)		10.5	8.9	8.5
Density ρ (g cm^{-3})		6.81	6.15	3.23
Melting point (K)		2146	2791	3487
Decomposition temperature (K)		630	850	1040
Binding energy (eV)		1.98	2.20	2.88

III-nitride device structures are generally grown on foreign substrates due to the lack of large-sized bulk GaN substrates, using metal organic chemical vapor deposition (MOCVD) and molecular beam epitaxy (MBE) techniques. The MOCVD and MBE techniques employ a high temperature process for III-nitride growth that limits the choice of substrate materials mostly to sapphire and Si due to their high thermal stability and commercial viability. The large lattice and thermal mismatch of GaN with sapphire and Si lead to generation of a high density of threading dislocations in the order of 10^8–10^{10} cm^{-2} in the grown GaN epitaxial layer [11–13]. The threading dislocations propagate from the GaN/substrate interface even to the surface deteriorating the optical and electrical properties of GaN based devices. Whereas, there are several other closely lattice- and thermal-matched substrates like $LiGaO_2$, ZnO, etc. available for GaN growth but they are vulnerable to higher growth temperatures above 600 °C. Therefore, development of a low temperature growth process is essential for group III-nitrides to further enhance their device performance. Laser molecular beam epitaxy (LMBE) is a relatively new technique for developing group III-nitride semiconductors but it can offer a low temperature growth process as the adequate kinetic energy for the precursors is supplied by the laser power itself. Low temperature growth of III-nitride epitaxial layers has already been demonstrated on various kinds of substrates including metals by using LMBE technique [14–18]. We have recently reported a low temperature growth of GaN layers on sapphire substrate by LMBE using laser ablation of liquid Ga and solid GaN targets under r.f. plasma ambient [19–24].

In recent years, GaN based nanostructures such as nanowires, nanorods, nanotubes and nanowalls are gaining a great research interest as they are dislocation-free and strain-free, and also have a large surface area-to-volume ratio. One dimensional (1D) nanostructures such as nanorods and nanotubes have enormous potential as fundamental building blocks for nanoscale electronic and optoelectronic devices. Few devices based on GaN 1D nanostructures such as field

effect transistors, p-n junctions, LEDs, Lasers and photo-detectors have been successfully demonstrated [25–29]. However, the fabrication of devices on individual 1D nanostructure is difficult due to the complications involved in their handling process. Here, two-dimensional (2D) nanowall network structures are convenient for the fabrication of nano-devices with their material continuity in the lateral direction and also show very interesting structural, optical and electrical properties. Especially, the electron mobility in c-axis oriented wedge-shaped GaN nanowall network grown on sapphire is estimated to be several orders of magnitude larger than that in GaN bulk and the electron mobility increases with the reduction of the average width of the wall [30, 31]. ZnO nanowall network based gas sensors, field emitters, and UV detectors have been reported in literature though GaN nanowall based devices are yet to be realized [32, 33].

Spontaneous formation of GaN nanowalls has been achieved by few researchers by using either plasma-assisted or ion-beam-assisted MBE techniques [30, 34, 35]. However, the growth of III-nitride nanostructures by LMBE technique is extremely limited [36]. In this chapter, we present the homo- and hetero-epitaxial growth of GaN nanowall network on GaN template and sapphire (0001) substrate using LMBE and discuss their structural, optical and electronic properties as characterized by various techniques.

9.2 Growth of GaN Nanowall Network by LMBE Technique

The growth of GaN nanowall network was carried out on 3.5 μm thick MOCVD grown GaN template on sapphire (0001) and bare sapphire (0001) substrates using an ultra-high vacuum (UHV) LMBE growth technique. The growth system was equipped with reflection high energy electron diffraction (RHEED) for in situ monitoring, residual gas analyzer and r.f. N_2 plasma source to supply additional nitrogen radicals. The base pressure of the LMBE growth chamber is $\sim 2 \times 10^{-10}$ Torr which is maintained by combination of various UHV pumps such as turbo molecular pump, titanium sublimation pump and ion pump. The schematic diagram of LMBE growth technique is represented in Fig. 9.1. A high quality HVPE grown solid, polycrystalline GaN target with a purity of 99.9999% was used as target material and semiconductor grade N_2 gas was used as the gas source in r.f. nitrogen plasma cell. A resistive heater was employed to raise the substrate temperature via infra red (IR) radiation. The back side of the GaN template and sapphire substrate was coated with a ~ 1 μm thick layer of molybdenum to increase the absorption of IR heat radiation and uniform heat distribution. The substrates were cleaned using standard organic solvents followed by de-ionized water. The substrates were initially heated in the entry load lock chamber for several hours at 200 °C to remove surface adsorbates and were then transferred into the growth chamber. The substrate temperature and the growth duration were kept

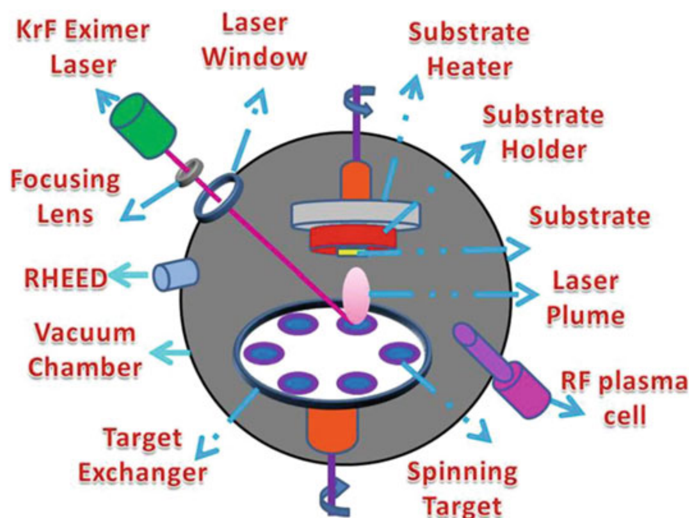

Fig. 9.1 Schematic diagram of laser molecular beam epitaxy (LMBE) growth technique

constant as 700 °C and 2 h, respectively. In case of sapphire substrate, it was thermally cleaned at 850 °C for 10 min in UHV condition followed by surface nitridation and GaN buffer growth at low temperature prior to the main GaN growth. A KrF excimer laser of 248 nm wavelength and 25 ns pulse width was used to ablate the GaN target with an energy density of $\sim$3 J/cm^2 and a laser repetition rate varying between 10 and 40 Hz. The r.f. nitrogen radicals were also supplied during the ablation of GaN target to provide N-rich growth condition for nanowall growth. The nitrogen gas flow and r.f. plasma power were fixed at 0.4 sccm and 250 W, respectively. The substrate cleaning and GaN growth were monitored in situ using RHEED operated at 25 kV. The effect of wet-etching on the GaN nanowalls grown on GaN template was also studied with KOH solution of 2M concentration for 30 min at room temperature.

9.3 Characterization of GaN Nanowall Network Grown by LMBE Technique

The structural properties of grown GaN samples were characterized using high resolution X-ray diffraction (HR-XRD) and Raman spectroscopy. The X-ray rocking curve (XRC) measurements along GaN (0002) and (10-12) planes were used to characterize the crystalline quality. The broadening of rocking curve is generally used to estimate the defects such as dislocation density and mosaic spread in the epitaxial layer. Here, the rocking curves of the GaN layers for (0002) and (10-12) diffraction planes were recorded in incident beam configuration using a

multilayer graded mirror with channel-cut 2-bounce Ge (220) monochromator using Cu Kα1 radiation. A scintillation detector was used to record the diffracted beam from the homo-epitaxial GaN for measurements of rocking curve. The micro-Raman spectra were collected in backscattering geometry using an excitation source of 514.5 nm wavelength. The plan- and 45° tilt-view surface morphologies of GaN nanowalls were analyzed by using a field-emission scanning electron microscopy (FE-SEM) with a 5 kV electron source.

The quantitative analysis of crystalline quality was also carried out using Rutherford backscattering geometry (RBS) technique. A well-collimated (divergence $\sim$0.05°) He^{++} ion beam of energy 3 meV from 1.7 MV Pelletron accelerator was used for the RBS/channeling measurements. The backscattered particles were detected using a surface barrier Si detector at an angle of 165° with respect to the incident beam. The optical emission properties were characterized using photoluminescence (PL) spectroscopy at room temperature with a 266 nm laser line as an excitation source. To investigate the electronic structures, X-ray photoelectron spectroscopy (XPS) measurements were carried out using monochromatic Al K_α and non-monochromatic dual anode (Al K_α and Mg K_α) X-ray sources housed in an UHV Multi Probe Surface Analysis System from Omicron at room temperature. An electrical contact was established between the sample surface and grounded sample plate with a highly conducting UHV compatible Ag paint in order to minimize charging during the XPS measurements of GaN nanowalls and GaN template samples. All binding energies have been referenced to the Fermi edge of an Ar+ sputtered clean polycrystalline Ag foil whereas charging correction was done using C 1s (284.8 eV) core-level binding energy [22]. Overall experimental energy resolution with 20 eV analyzer pass energy for monochromatic Al Kα (1486.7 eV) and non-monochromatic Mg Kα (1253.5 eV) is 0.45 and 0.9 eV, respectively [22].

9.4 Properties of Homoepitaxial GaN Nanowall Network Grown on GaN Template

9.4.1 Structural Properties

The cleaning of GaN template and LMBE growth of GaN were monitored by in situ RHEED technique. The RHEED observation of GaN template showed a streaky pattern along [11-20] and [10-10] directions as presented in Fig. 9.2a, which is the sign of an atomically flat surface suitable for epitaxial growth. During the LMBE GaN growth, the streaky pattern changed to aligned spotty features indicating an epitaxial three-dimensional (3D) growth of GaN under the adopted experimental conditions and the respective RHEED patterns are given in Fig. 9.2b. The twist and tilt in the GaN template and LMBE GaN were examined using symmetric and asymmetric XRC measurements, respectively. The symmetric (0002) plane and asymmetric (10-12) plane XRCs of GaN template are presented in Fig. 9.3. The full

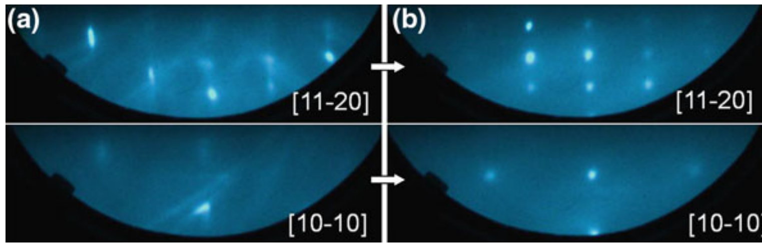

Fig. 9.2 RHEED patterns of **a** GaN template and **b** homoepitaxial GaN growth during LMBE technique, taken along [11-20] and [10-10] directions

width at half maximum (FWHM) of XRC is an indication of crystalline quality of the grown layers. The XRC FWHM values of (0002) and (10-12) planes of GaN template was obtained as 292 and 375 arc-sec, respectively, whereas, the values increased to 310 and 436 arc-sec for the LMBE grown GaN at 10 Hz. The values further increased as a function of laser repetition rate as shown in Fig. 9.4. A maximum of 320 and 468 arc-sec were obtained along (0002) and (10-10) planes for the GaN grown at 30 Hz (the respective XRCs are shown in Fig. 9.3). These observations exhibit that the crystalline quality of GaN is slightly distorted during LMBE growth especially at higher laser repetition rates up to 30 Hz. However, the asymmetric XRC FWHM value decreased significantly for the LMBE GaN grown at 40 Hz.

Surface morphology of the LMBE grown GaN samples on GaN template were characterized by FESEM and the plan- and and 45° tilted-view FESEM images are shown in Fig. 9.5. For the GaN grown at the low repetition rate of 10 Hz, highly dense, un-coalesced GaN islands are observed. The respective 45° tilt-view FESEM image shows an elongated GaN growth in the lateral direction as in Fig. 9.5a. Further increase in the laser frequency to 20 Hz leads to the formation of GaN nanowall network structure with a large number of hexagonal-shaped pores of size ranging from 90 to 120 nm. The nanowall width is tapered from the base towards the top with a tip width of about 20–30 nm as seen in Fig. 9.5b. The well-defined GaN nanowall network with a pore size of 120–180 nm has been observed for 30 Hz growth (Fig. 9.5c). The individual GaN nanowalls have a tip width of about 10–15 nm that overlap and interlace with one another to form a continuous network structure. In comparison, the pore size of the GaN nanowall network increased with increasing laser repetition rate from 20 to 30 Hz while the tip width decreased dramatically. For 40 Hz growth, the GaN layer of coalesced islands has been obtained with presence of a high density of surface pits. The surface pits are inverted hexagonal pyramids formed due to the remnants of island coalescence process and are characteristics of GaN growth.

Growth mode of GaN based materials shows a sharp sensitivity to the Ga/N flux ratio prevailing on the growth front. Under Ga-rich flux condition, i.e. N/Ga ratio <1, GaN grows in 2D mode yielding an atomically flat surface while N-rich condition with N/Ga ratio >1 mostly promotes a 3D growth of rough surface [37, 38].

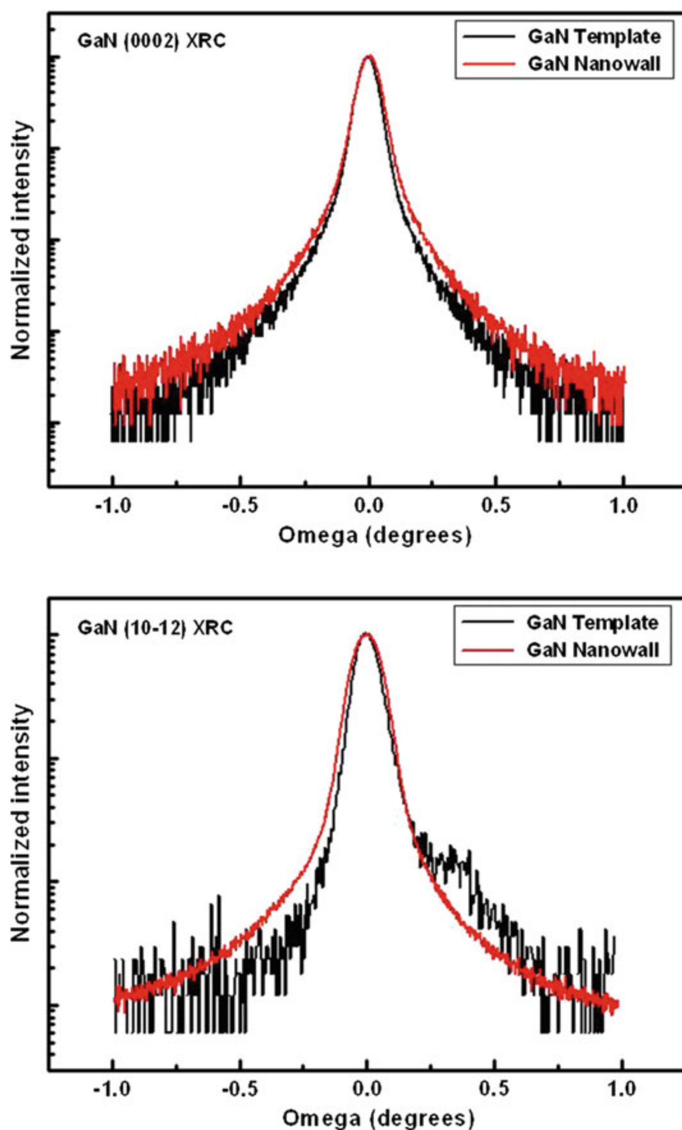

Fig. 9.3 High resolution X-ray rocking curves of GaN template and GaN nanowalls grown at 30 Hz: **a** (0002) and **b** (10-12) planes

The nanowall network is basically a vertically grown structure and the researchers have obtained growth of GaN nanowall network on different substrates under a highly nitrogen-rich flux condition using conventional MBE technique [34, 39–42]. Zhong and Hane have studied the effect of Ga/N flux ratio on the growth of GaN on Si (111) substrate by varying the N to Ga ratio from 180 to 980. The nanowall

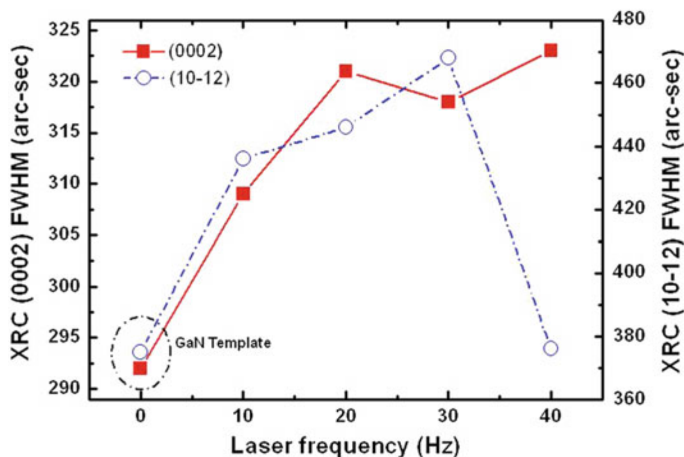

Fig. 9.4 X-ray rocking curve full width at half maximum (FWHM) of GaN template and LMBE grown GaN as a function of laser frequency

width could be controlled from 30 to 200 nm by adjusting the N/Ga flux ratio in the above range [34]. Poppitz et al. achieved growth of porous GaN nanowall network on SiC using ion-beam-assisted MBE in the temperature range 750–850 °C by keeping the N ion to Ga atom ratio between 2.7 and 6.3 [35]. Spontaneous growth of GaN nanowalls on sapphire (0001) has been reported under the N/Ga ratio of 100 by Kesaria et al. [39]. In the LMBE growth of GaN nanowall, the in situ RHEED showed the 3D growth with a spotty pattern indicating the N-rich flux condition.

Based on the experimental conditions and the observed results, a possible growth mechanism can be proposed for GaN nanowall network structure. As discussed earlier, the available reports unanimously suggest that nitrogen-rich growth condition is the most fundamental requirement for the formation of GaN nanowall structure. In addition, the large lattice and thermal mismatch between GaN and foreign substrates like sapphire and Si are also considered to understand the growth mechanism of nanowall structure as the relative biaxial stress can relax via formation of 3D structures [34, 39–42]. However, in case of GaN nanowall growth on thick GaN template, the contribution of in-plane stress will be a minimum. Hence, the growth mechanism of LMBE grown homoepitaxial GaN nanowall network can be understood on the basis of N-rich growth condition and high flux rates. In LMBE GaN growth, the laser ablation process of solid polycrystalline GaN target was carried out under the r.f. activated nitrogen plasma ambient, which is a N-rich flux situation prone for 3D growth. In addition, the surface kinetics of adatoms should also be considered as the increase in flux rate greatly influences the growth process of epitaxial layers. When the laser frequency is increased from 10 to 40 Hz, there is a multifold increase of flux rate for the GaN growth. While the low flux rate at 10 Hz results in un-coalesced GaN islands the high flux at 40 Hz leads to formation of a coalesced layer with a high density of large pits. The GaN nanowall network

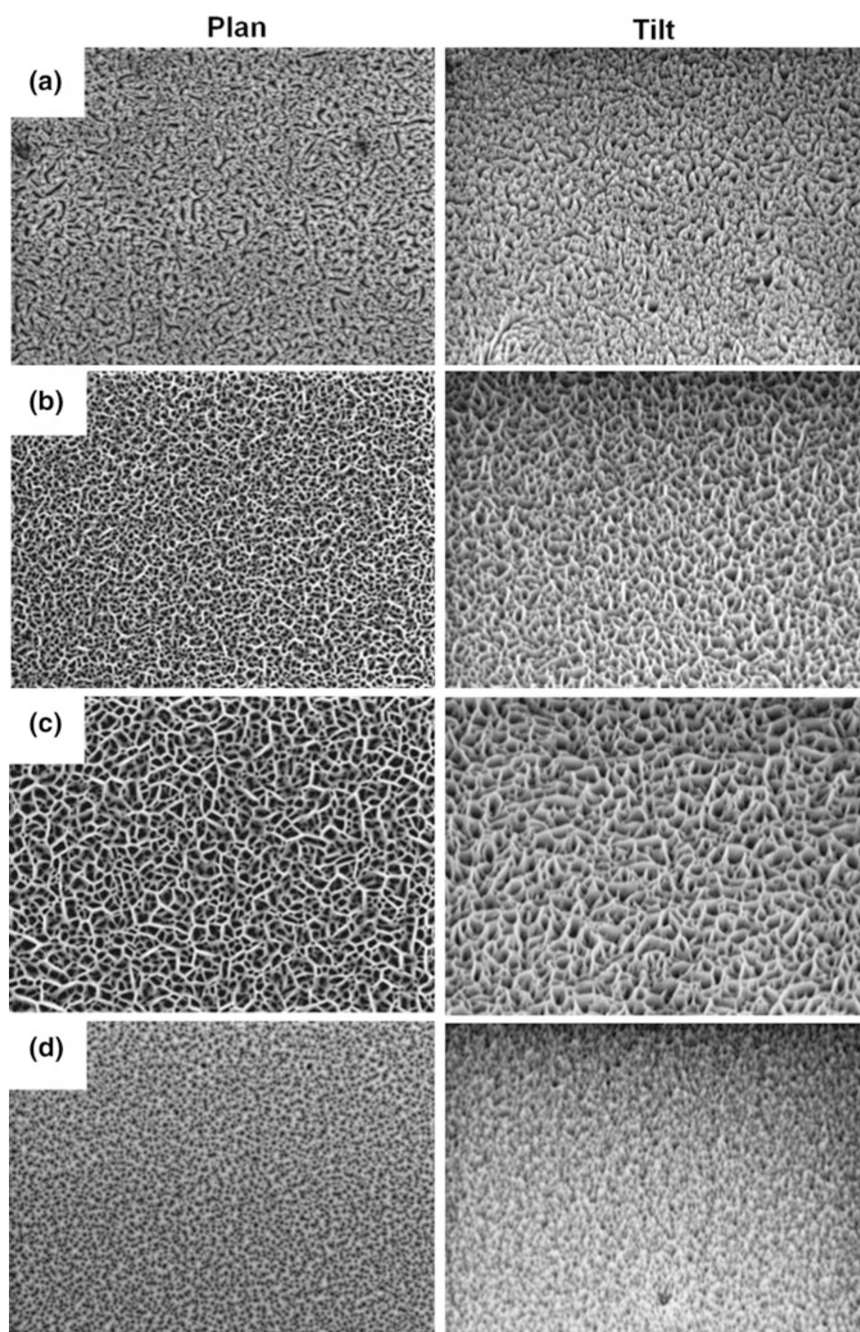

Fig. 9.5 Plan- and 45° tilt-view FESEM images of GaN structures grown on GaN template at various laser frequencies: **a** 10 Hz, **b** 20 Hz, **c** 30 Hz and **d** 40 Hz

structures are obtained only for the intermediate flux rates at 20–30 Hz. With increase in flux rate, the diffusion length of surface adatoms decreases due to limited surface mobility by impinging flux, which sets on a vertical growth. At 10 Hz, the flux is not sufficient to form a continuous layer in the designated growth duration of 2 h. At intermediate flux conditions i.e., 20 and 30 Hz, the GaN nanowall network is formed due to diffusion limited vertical growth in the lateral direction, which leads to nanowall formation. High density GaN nucleation islands due to higher flux rate at 40 Hz tend to form a layer structure by early coalescence among them. From the statistical analyses of nanowall network dimensions obtained for 20 and 30 Hz, it is understood that the increase of pore size at higher frequency occurs due to low surface diffusion of GaN adatoms by the increased flux rate. Moreover, the sticking coefficient of Ga atoms is relatively higher at GaN (0001) plane compared to other planes, which can further contribute towards the 3D growth [42, 43]. The above results are evident that GaN nanowalls could be grown homoepitaxially on GaN template at higher flux rates under N-rich flux condition using LMBE technique.

Raman spectroscopy has been applied to evaluate the crystalline quality and the presence of in-plane strain in the LMBE grown GaN structures. The Raman spectra of GaN grown at various laser frequencies were recorded at room temperature in backscattering geometry and are presented in Fig. 9.6. GaN normally crystallizes in hexagonal wrutzite structure and the Raman active modes of wurtzite GaN are A_1 (LO), A_1 (TO), E_1 (LO), E_1 (TO), E_2 (low) and E_2 (high). According to Raman selection rules, only E_2 (high) and A_1 (LO) phonon modes are expected in the backscattering geometry with laser beam incident on GaN (0001) surface.

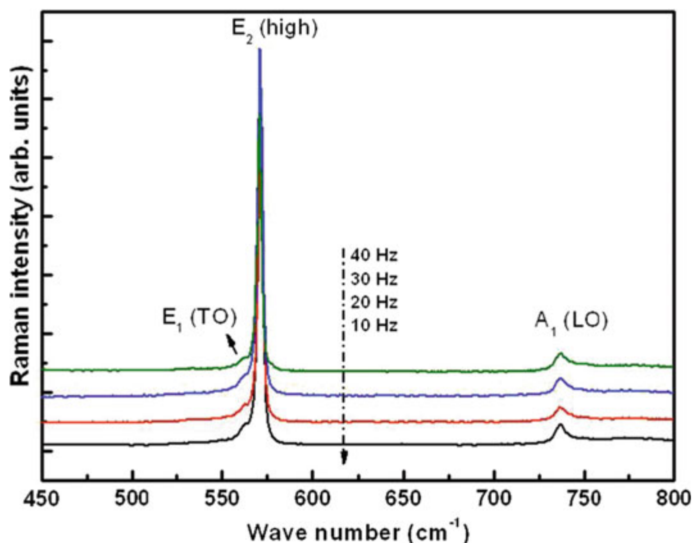

Fig. 9.6 Room temperature Raman spectra of LMBE grown GaN at various laser frequencies

By analyzing the line shape, FWHM value and shift of E_2 (high) peak, the crystalline quality and the in-plane stress/strain in the GaN layer can be accessed while the A_1 (LO) mode gives information on the carrier concentration and electron mobility [44, 45]. For the LMBE GaN, a strong E_2 (high) mode and A_1 (LO) mode are seen at 571.3 and 736.8 cm^{-1}, respectively. Compared to the E_2 (high) position of stress-free GaN at 567.6 cm^{-1}, a peak shift of about 3.7 cm^{-1} has been obtained for GaN template as well as LMBE grown GaN structures indicating a presence of in-plane compressive strain [46]. It is noted that there is no change in the intrinsic strain of the template over LMBE growth of GaN. The position and width of GaN Raman modes of all samples have been analyzed with Lorentzian peak fit. It is found that the peak position and FWHM of both E_2 (high) and A_1 (LO) modes remain almost same with increase of laser frequency from 10 to 40 Hz. There is a shoulder peak near E_2 (high) mode at 561.8 cm^{-1}, which is assigned to E_1 (TO) mode. The peak width of E_1 (TO) mode monotonically varies from 6.0 to 11.2 cm^{-1} with increase of frequency from 10 to 40 Hz. The increase of FWHM value of E_1 (TO) mode with respect to laser frequency indicates the increased structural defects as in good agreement with HRXRD analysis.

Rutherford backscattering experiments were performed to characterize the crystalline nature of the GaN nanowall network structure. The RBS/ion channeling spectra of GaN template and LMBE grown GaN nanowall network structures are given in Fig. 9.7. The ion channeling yield (the ratio of the backscattering yield of aligned direction to that from the random direction in the near surface region) is very low about 3.2% for the GaN template. The low RBS yield in the aligned direction is an indication of the high crystalline order of the grown GaN layer that is revealing the very high order of lattice arrangements. The ion channeling yield for the GaN nanowall network structures increased to 9.8% indicating a slight disorder of crystallinity during LMBE growth. The RBS observation is consistent with the HRXRD and Raman data.

9.4.2 Optical Properties

Optical emission properties of the LMBE grown GaN structures in the frequency range 10–40 Hz have been characterized by room temperature PL measurements and the respective PL spectra are presented in Fig. 9.8. The PL data were acquired under the same measurement parameters such as incident beam aperture size and laser power for all samples. In common, a strong UV emission at $\sim$362 nm (3.43 eV) and a broad, weak deep-band emission centered at the wavelength of 540 nm (2.30 eV) are obtained for the GaN template and LMBE grown GaN samples. Bulk wurtzite GaN exhibit a near band edge (NBE) emission at $\sim$3.4 eV and defects related peaks in the range of 1.4–2.8 eV at room temperature [47]. The shift in NBE position compared to bulk GaN is related to the stress present in the GaN template itself. It has been observed that the E_2 (high) Raman shift of 4.2 cm^{-1} due to biaxial stress in GaN layer makes a 27 meV of blue shift in NBE peak

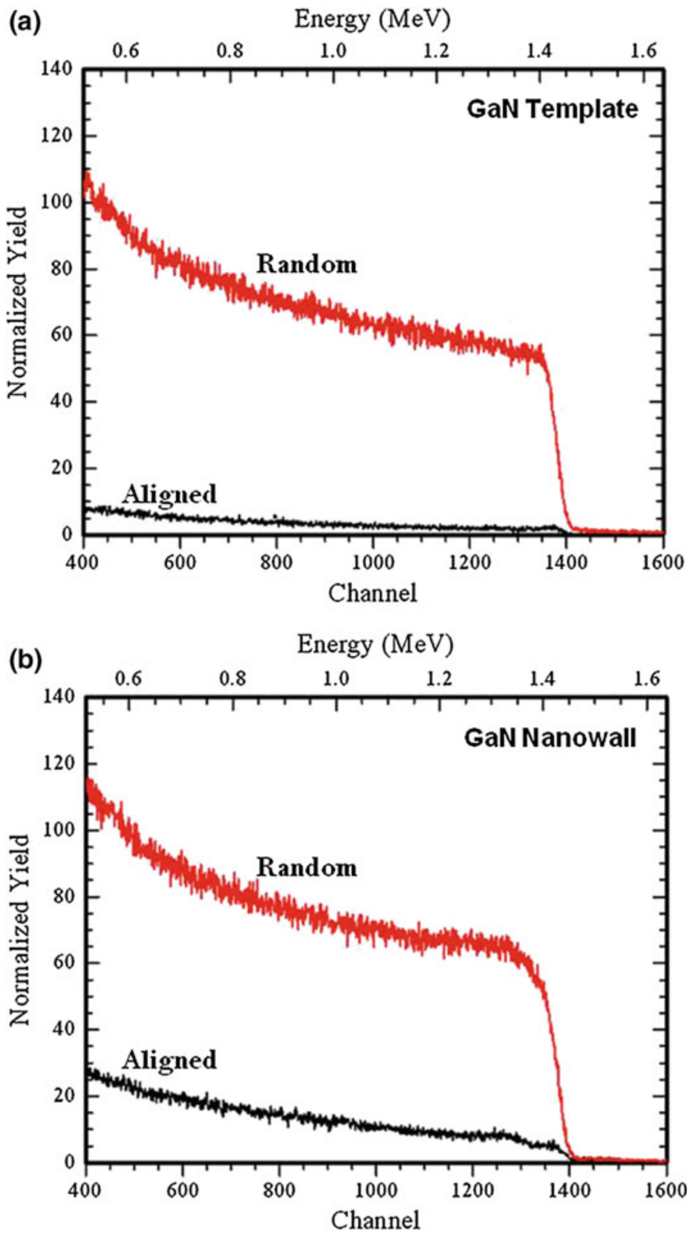

Fig. 9.7 Rutherford backscattering spectroscopy of **a** GaN template and **b** LMBE grown GaN nanowall network structure

position [24, 46]. The deep band emission is the characteristic yellow luminescence (YL) of GaN associated with intrinsic crystalline defects. The contribution of GaN template in the PL data of LMBE GaN samples is possible and the obtained PL data for all the samples cab be the combined effect of the template and the LMBE grown GaN. At the same time, the notable change in the spectral features and NBE/YL intensity ratio can provide information on the optical properties of the LMBE grown GaN. The NBE/YL intensity ratio of the template and LMBE grown GaN at 10, 20, 30 and 40 Hz are obtained to be 43, 37, 18, 17 and 11, respectively. Compared to GaN template, the ratio decreased as a function of laser frequency. It indicates the generation of structural defects during LMBE growth, which are responsible for YL emission [48]. In the literature, there are contradictory results about the presence of YL peak intensity in GaN nanowall network. While few reports claim a negligible YL emission for GaN nanowall network [41, 49], some researchers observed prominent defect related peaks [42, 48].

For the GaN nanowall network structure grown at 30 Hz, an additional peak at the higher energy region above NBE is observed as noted in the respective PL spectrum. To analyze the higher energy emission, the PL data was fitted using Lorentzian function and the position of new emission peak is identified to be 352 nm (3.52 eV). It should be mentioned that the higher energy peak with a blue shift of 90 meV from NBE emission is observed only for the GaN nanowalls network having a tip width of 10–15 nm. The GaN nanowall network with tip width of 20–30 nm grown at 20 Hz did not exhibit any higher energy emission. Recently, Bhasker et al. have reported that the NBE of GaN nanowalls of tip width $\sim$10 nm is shifted by 60 meV towards higher energy side compared to that of the

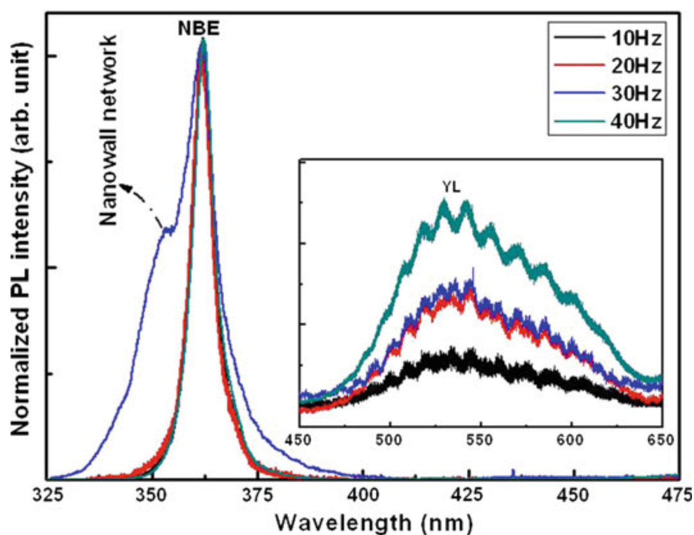

Fig. 9.8 Room temperature photoluminescence spectra of LMBE grown GaN at various laser frequencies (*Inset* yellow luminescence)

GaN epitaxial layer and the enhancement of the band gap was explained on the basis of carrier confinement effect in the nanowall structures [49]. Similarly, in case of ZnO nanowalls grown on GaN template, the room temperature PL spectrum showed a blue shift of NBE attributed to the quantum confinement effect [50]. GaN nanowires of diameter comparable to Bohr exciton radius of GaN, i.e., $\sim$11 nm, also exhibited a PL blue shift induced by quantum confinement effect induced [51]. Similarly, in the LMBE grown GaN nanowalls, the higher energy PL peak is observed for wall width of 10–15 nm that is comparable to the Bohr exciton radius of GaN. Therefore, the PL emission at 3.52 eV of GaN nanowall network is assigned to quantum confinement of the charge carriers [36].

9.4.3 Electronic Structure

The electronic structure of GaN template and GaN nanowall network were characterized using XPS studies [36]. Also, the XPS core level spectroscopy is one the most powerful technique to determine the surface chemical composition. A monochromatic Al K_α source was employed to study the Ga 3d core level as it is free from additional X-ray satellites and offers a high energy resolution better than non-monochromatic X-ray source. But, at the same time, it makes the N 1s core level analysis more complicated as the N 1s spectrum overlaps with the broad Ga Auger features and is not suitable to determine the chemical composition of GaN. Hence, N 1s core level data was acquired using a non-monochromatic Mg K_α source as the Ga Auger features do not overlap with the N 1s core level any more [22]. The Ga 3d and N 1s core level spectra of GaN template and GaN nanowall network measured using Al Kα and Mg Kα sources, respectively, are shown in Fig. 9.9a, b. To determine accurate peak positions and relative contribution of different components, the χ^2 iterative fit of Ga 3d and N 1s core level spectra were carried out. Ga 3d core level spectra of GaN template can be fitted using 3 components such as Ga–N, Ga–O, and N 2s while the fitting of Ga 3d core level spectrum of GaN nanowall network was done with 4 components, i.e. with an additional Ga–Ga component. As seen, in both cases, the Ga 3d core level spectrum is mainly dominated by Ga–N peak which appears at 19.95 $\pm$ 0.05 eV for GaN template and at 20.1 $\pm$ 0.05 eV for GaN nanowall network. The peak position and FWHM values for GaN template are close to the earlier reports [52, 53]. The FWHM is relatively large for the GaN nanowall network. Ga–O component, assigned to the formation of Ga_2O_3, is observed at 1.2 eV higher binding energy (BE) side compared to main peak. It might be due to surface oxidation of GaN upon exposure to atmospheric ambient [54, 55]. Ga–Ga component is located at 1.0 eV lower BE side compared to main peak and it can be related to uncoordinated/metallic Ga atoms [53, 54]. Relative percentage of Ga–O varies very little (7.2–7.9) between the GaN template and the nanowall network indicating a similar amount of surface oxidation.

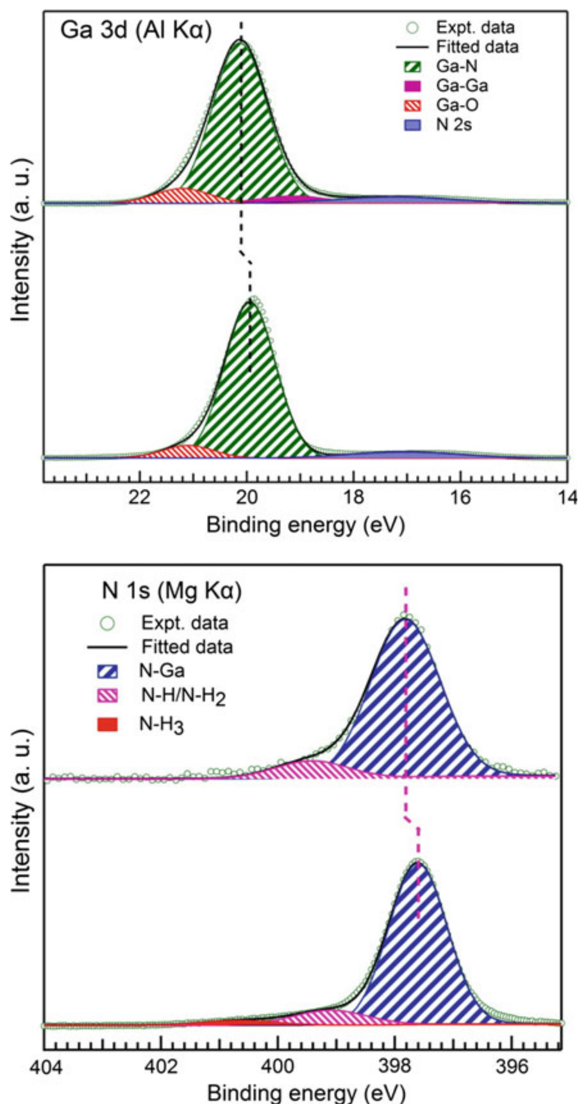

Fig. 9.9 X-ray photoemission spectra of GaN template and GaN nanowall network: Ga 3d and N 1s core levels

In case of N 1s core level, the spectra can be fitted by 2 components such as major N–Ga and surface contamination related N–H/N–H_2 peaks. The N–Ga peak dominates the spectra and N–H/N–H_2 component appears at 1.5 eV higher BE side [53, 56]. For the GaN template, a small feature at 3.0 eV higher BE side is obtained and can be attributed to NH_3 contamination occurred during MOCVD growth [56]. N–Ga peak for GaN template and nanowall network appear at 397.6 ± 0.05 and 397.8 ± 0.05 eV, respectively. To calculate the surface chemical composition of the GaN, area under the curve of Ga 3d and N 1s core levels have been normalized

using respective photo-ionization cross sections, inelastic mean free path and analyzer transmission function [22, 57, 58]. The Ga/N ratio for GaN template and GaN nanowall network are calculated to be 1.04 ± 0.05 and 2.03 ± 0.1, respectively. It clearly indicates that the LMBE grown GaN nanowall network is rich in Ga content. It has been reported that Ga-rich surface may result due to formation of Ga adlayer and/or Ga droplets and it can result in surface reconstructions [59–61]. Surface sensitivity of XPS can be tuned by varying the photoemission angle. From angle dependent photoemission measurements, the Ga/N ratio was found to be nearly same within the experimental error and therefore, the possibility of excess Ga at nanowall surface can be excluded [36]. The large Ga/N ratio of the LMBE grown GaN nanowall network suggests that it will have a large number of N vacancy related defects; it can be correlated with the more defective nature of the LMBE grown GaN as observed by the large X-ray rocking width and the enhanced peak intensity of YL band in PL spectrum [62]. Ga 3d and N 1s core levels of the GaN nanowall network shifts towards higher BE side by 0.15–0.2 eV, respectively, compared to the GaN template and such shifts have been attributed to the presence of N vacancies in GaN [63–66]. In recent past, N vacancies have emerged as major point defect in bulk and nanostructured GaN [67–69]. Fitting of Ga 3d core level spectrum of the LMBE grown nanowall network also confirmed the formation of uncoordinated Ga atoms, possibly located at interstitial sites, pointing towards the presence of N vacancies.

The VB spectra of GaN template and LMBE grown GaN nanowall network measured using Al K_{α} source are given in Fig. 9.9. The VB spectra can be satisfactorily fitted using 3 components corresponding to features A, B and C. The peaks A and C are associated to Ga 4p-N 2p and Ga 4s-N 2p hybridized states, respectively, with N 2p dominant character and the peak B has been attributed to mixed orbitals and/or surface adsorbates [70]. For the GaN template, the features A, B and C appeared at 4.5 ± 0.5, 6.92 ± 0.5, and 9.1 ± 0.5, respectively. Line shape and energy position of dominant features of the VB spectra are in good agreement with the earlier reports [70–72]. Similar to Ga 3d and N 1s core levels, the FWHM of VB peaks for GaN nanowall network are found to be higher compared to GaN template which could be correlated to the increased structural defects. Also, there is a very small shift of A and C peaks towards higher BE for the GaN nanowalls with respect to GaN template. These observations indicate that a redistribution of spectral weight takes place in GaN nanowall and it can be attributed to the change in Ga/N ratio and the consequent change in Ga–N hybridization.

The near E_F VB spectra of GaN template and nanowalls are presented in Fig. 9.10. The position of valence band maxima (VBM) has been found to lie at 2.67 ± 0.05, and 2.78 ± 0.05 eV below the surface Fermi level for GaN template and GaN nanowall network, respectively. Since GaN has a bandgap of about 3.4 eV at room temperature the VBM positions indicate that GaN template and nanowalls have n-type electrical conductivity. Also, in comparison with GaN template, the VBM of GaN nanowall network is shifted by ~0.1 eV towards higher BE, which may be correlated to the increase in band gap as revealed by room temperature PL. In contrast, the N vacancy induced change in surface band bending

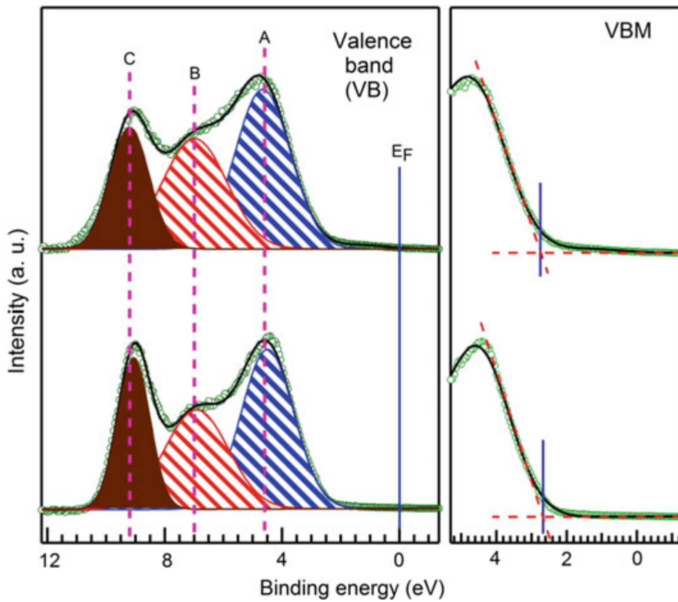

Fig. 9.10 X-ray photoemission valence band spectra of GaN template and GaN nanowall network

may also shift VBM and Ga 3d and N 1s core levels. N vacancy related donor states may increase near surface electron concentration resulting in positive surface charge that will result in a reduction of positive space charge in the depletion region and lower the band bending. In addition the surface oxidation level of GaN can also affect the VBM and core level BE [73]. As the surface oxidation level is similar in GaN template and nanowalls the related effect on peak shift would be insignificant. It is noted that any evidence of presence of metallic states related to uncoordinated Ga atoms is not found as there is no spectral weight around E_F.

9.4.4 Effect of Wet-Etching

The surface morphology of wet-etched GaN nanowall network grown at 30 Hz is shown in Fig. 9.11. The room temperature KOH wet-etching largely modifies the GaN nanowall structure. The sharp edge and pore areas of the nanowall network are etched-out thereby increasing the nanowall edge width and pore size. In addition, numerous, small-sized pores are newly revealed in the surface.

The room temperature PL spectra of GaN nanowall network before and after wet-etching are given in Fig. 9.12. After the wet-etching, the higher energy PL emission peak at ~3.52 eV assigned to the GaN nanowall network totally disappeared from the spectrum. The GaN NBE peak becomes sharper and the YL

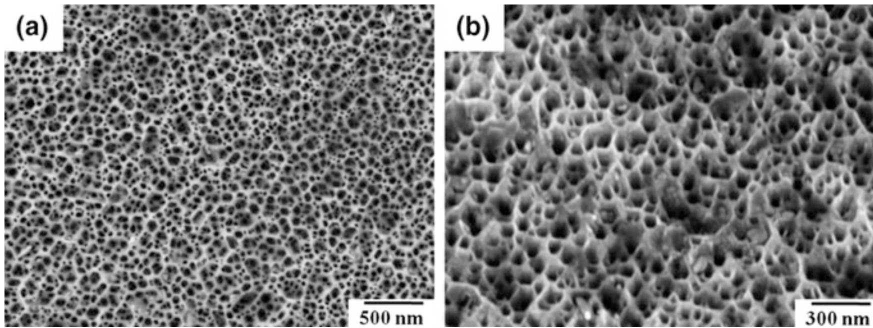

Fig. 9.11 **a** Plan- and **b** 45° tilt-view FESEM images of wet-etched GaN nanowall network structure

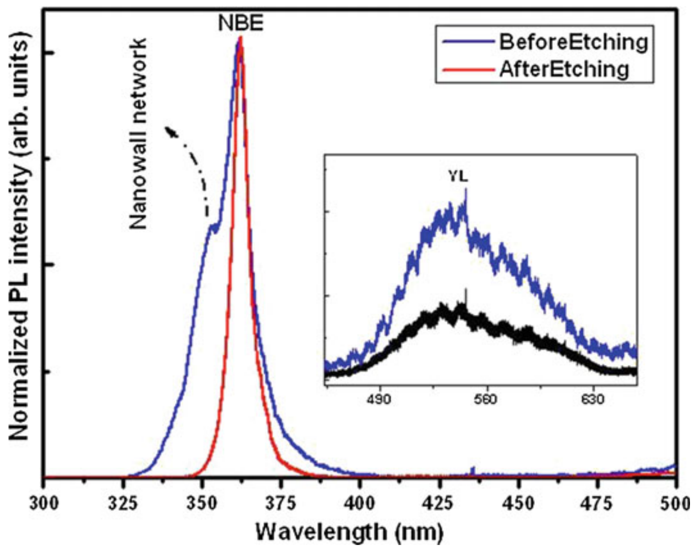

Fig. 9.12 Room temperature photoluminescence spectra of as-grown and wet-etched GaN nanowall network structure (*Inset* yellow luminescence)

emission intensity is also reduced. The NBE/YL intensity ratio increased from 20 to 41 after etching. The absence of higher energy peak above NBE confirms that the emission at ~3.52 eV belongs to the GaN nanowalls due to quantum confinement effect. The reduction of NBE peak width and YL intensity of wet-etched GaN nanowalls are attributed to the removal of relatively defective LMBE grown GaN material.

9.5 Properties of Heteroepitaxial GaN Nanowall Network Grown on Sapphire (0001)

Growth of heteroepitaxial GaN nanowall network structure has been achieved on pre-nitridated sapphire substrate under similar experimental conditions employed for the growth on GaN template by LMBE. Only, the laser frequency and growth time were maintained as 10 Hz and 3 h, respectively. The in situ RHEED patterns recorded after sapphire cleaning and during GaN growth are given in Fig. 9.13. The RHEED indicated a clean and atomically flat sapphire surface with short streaky features. The RHEED obtained during GaN growth revealed a 3D growth of GaN with 30° in-plane rotation with respect to sapphire substrate [74]. Figure 9.14 shows the surface morphology of heteroepitaxial GaN nanowall network in plan- and 45° tilt-views. The nanowall network formation is analogous to that grown on GaN template. The nanowalls have a tip width of 9–20 nm and a pore size of 50–120 nm.

The room temperature photoluminescence spectrum of GaN nanowalls grown on sapphire substrate is presented in Fig. 9.15. A strong UV emission around 3.5 eV (~355 nm) related to GaN nanowalls appeared with a blue shift of about 100 meV

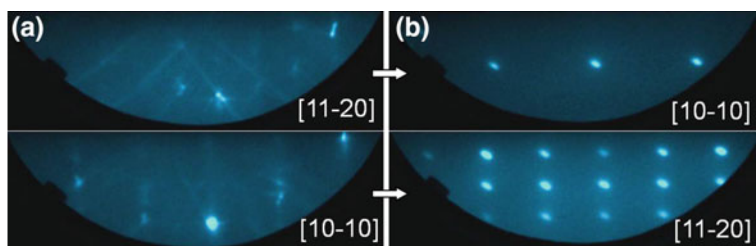

Fig. 9.13 **a** RHEED patterns of (**a**) thermally cleaned sapphire (0001) substrate and **b** heteroepitaxial GaN nanowall growth during LMBE, taken along [11-20] and [10-10] directions

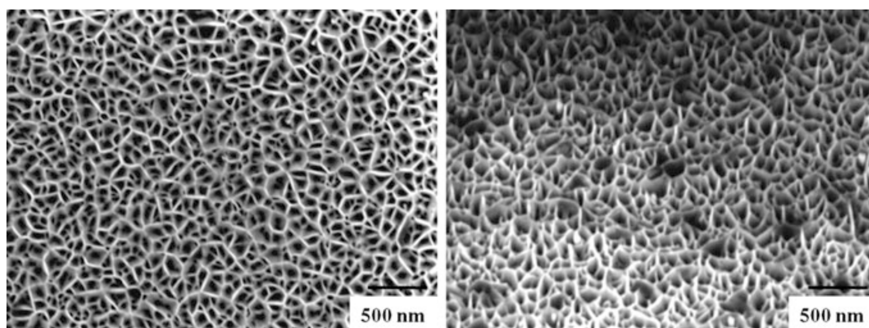

Fig. 9.14 Plan and 45° tilt view FESEM images of heteroepitaxial GaN nanowall network grown on sapphire (0001) substrate

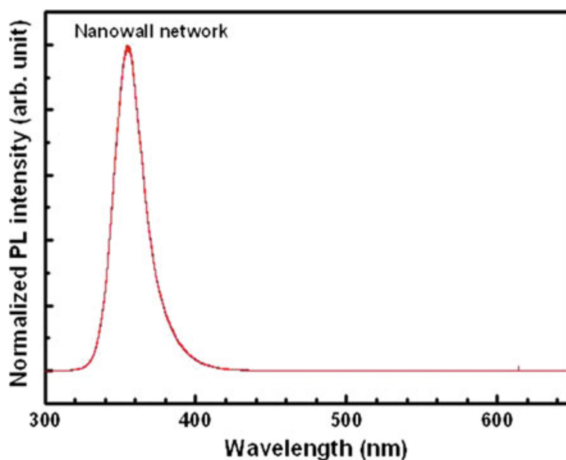

Fig. 9.15 Room temperature photoluminescence spectrum of heteroepitaxial GaN nanowall network grown on sapphire (0001) substrate

from the band energy of bulk GaN. The higher energy emission is due to the carrier confinement in nanowall edges of thin width comparable to Bohr radius of GaN as discussed in the previous section. The YL band intensity is found to be negligible, which denotes the good structural properties of the grown GaN nanowalls. Thus, the LMBE growth technique demonstrates a great promise for producing homo- and hetero-epitaxial GaN nanowall network under suitable experimental conditions that can be employed in realizing nitride nano-devices for various unique applications [32, 33, 75].

9.6 Concluding Remarks and Future Perspective

Homoepitaxial GaN nanowall network were grown on GaN template by laser ablation of solid GaN target in presence of r.f. nitrogen plasma by using LMBE technique. The role of laser frequency is found to be critical in the formation of GaN nanowall structure in LMBE growth. The GaN nanowall width decreases as a function of laser frequency and nanowall network with edge width of 10–15 nm and pore size of 120–180 nm are obtained at 30 Hz. The structural, electronic and optical properties of the GaN nanowall structures have been characterized. HRXRD, Raman and RBS studies indicate that the crystalline quality of LMBE grown GaN nanowalls are slightly changed as compared to that of MOCVD grown GaN template. The room temperature PL measurement shows a high energy emission from GaN nanowall network at 3.52 eV due to the quantum confinement of carriers at the nanowall edges. An increased width of GaN nanowall has been obtained after a wet-chemical etching in KOH and consequently, the nanowall related PL emission disappeared confirming the presence of quantum confinement effect only in thinner nanowall structures. Heteroepitaxial GaN nanowall network of

edge with <15 nm were also grown on sapphire (0001) substrate by LMBE. A higher energy PL emission from the heteroepitaxially grown nanowall is obtained around 3.5 eV at room temperature due to carrier confinement. Similar to conventional MBE, N-rich flux condition is found to be favorable to achieve GaN nanowall network structure by LMBE growth.

The LMBE grown GaN nanowall network with a large surface area and confined charge carriers will have potential technological applications in the area of field emission and high temperature sensing. The porous network structure can also be used for surface texturing of light emitters and solar cells to improve their output efficiency.

Acknowledgements The authors would like to thank Dr. K.K. Maurya, Dr. Ajay K. Shukla, Dr. Dilip K. Singh, Ms. Mandeep Kaur, Dr. B.S. Yadav (SSPL, Delhi) and Mr. Sunil Ojha (IUAC, New Delhi) for the assistance in sample characterizations. The financial support by Council of Scientific and Industrial Research (CSIR) through network project PSC-0109 is also gratefully acknowledged.

References

1. S. Nakamura, T. Mukai, M. Senoh, Candela-class high-brightness InGaN/AlGaN double heterostructure blue light emitting diodes. Appl. Phys. Lett. **64**, 1687 (1994)
2. S. Nakamura, M. Senoh, S. Nagahama, N. Iwasa, T. Yamada, T. Matsushita, H. Kiyoku, Y. Sugimoto, T. Kozaki, H. Umemoto, M. Sano, K. Chocho, Continuous-wave operation of InGaN/GaN/AlGaN based laser diodes grown on GaN substrates. Appl. Phys. Lett. **72**, 2014 (1998)
3. F.A. Ponce, D.P. Bour, Nitride-based semiconductors for blue and green light-emitting devices. Nature **386**, 351 (1997)
4. S. Nakamura, G. Fasol, *The Blue Laser Diode—GaN Based Light Emitters and Lasers* (Springer, Berlin, 1997)
5. S.C. Allen, A.J. Steck, A nearly ideal phosphor-converted white light emitting diode. Appl. Phys. Lett. **92**, 143309 (2008)
6. J. Wu, When group-III nitrides go infrared: new properties and perspectives. J. Appl. Phys. **106**, 011101 (2009)
7. H. Morkoc, *Nitride Semiconductors and Devices* (Springer, New York, 1999)
8. O. Ambacher, Growth and applications of group III-nitrides. J. Phys. D Appl. Phys. **31**, 2653 (1998)
9. M. Shur, B. Gelmont, M.A. Khan, Electron mobility in two-dimensional electron gas in AIGaN/GaN heterostructures and in bulk GaN. J. Electron. Mater. **25**, 777 (1996)
10. T. Brazzini, M.A. Casbon, H. Sun, M.J. Uren, J. Lees, P.J. Tasker, H. Jung, H. Blanck, M. Kuball, Electroluminescence of hot electrons in AlGaN/GaN high-electron-mobility transistors under radio frequency operation. Appl. Phys. Lett. **106**, 213502 (2015)
11. H.-Y. Shin, S.K. Kwon, Y.I. Chang, M.J. Cho, K.H. Park, Reducing dislocation density in GaN films using a cone-shaped patterned sapphire substrate. J. Cryst. Growth **311**, 4167 (2009)
12. V.E. Bougrov, M.A. Odnoblyudov, A.E. Romanov, T. Lang, O.V. Konstantinov, Threading dislocation density reduction in two-stage growth of GaN layers. Phys. Stat. Sol. (a) **203**, R25 (2006)

13. X. Weng, J.D. Acord, A. Jain, E.C. Dickey, J.M. Redwing, Evolution of threading dislocation density and stress in GaN films grown on (111) Si substrates by metalorganic chemical vapor deposition. J. Electron. Mater. **36**, 346 (2007)
14. K. Okamoto, S. Inoue, N. Matsuki, T.-W. Kim, J. Ohto, M. Oshima, H. Fujioka, A. Ishii, Epitaxial growth of GaN films grown on single crystal Fe substrates. Appl. Phys. Lett. **93**, 251906 (2008)
15. A. Kobayashi, S. Kawano, K. Ueno, J. Ohta, H. Fujioka, H. Amani, S. Nagao, H. Horie, Growth of a-plane GaN on lattice-matched ZnO substrates using a room-temperature buffer layer. Appl. Phys. Lett. **91**, 191905 (2007)
16. K. Sakurada, A. Kobayashi, Y. Kawaguchi, J. Ohta, H. Fujioka, Low temperature epitaxial growth of GaN films on $LiGaO_2$ substrates. Appl. Phys. Lett. **90**, 211913 (2007)
17. Y. Kawaguchi, J. Ohta, A. Kobayashi, H. Fujioka, Room-temperature epitaxial growth of GaN on lattice-matched ZrB_2 substrates by pulsed-laser deposition. Appl. Phys. Lett. **87**, 221907 (2005)
18. R.D. Vispute, V. Talyansky, R.P. Sharma, S. Choopun, M. Downes, T. Venkatesan, K.A. Jones, A.A. Iliadis, M. Asif Khan, J.W. Yang, Growth of epitaxial GaN films by pulsed laser deposition. Appl. Phys. Lett. **71**, 102 (1997)
19. M. Senthil Kumar, S.S. Kushvaha, K.K. Maurya, Low temperature growth of GaN epitaxial layers on sapphire (0001) by pulsed laser deposition using liquid Gallium target. Sci. Adv. Mater. **6**, 1215 (2014)
20. S.S. Kushvaha, M. Senthil Kumar, K.K. Maurya, M.K. Dalai, N.D. Sharma, Highly c-axis oriented growth of GaN film on sapphire (0001) by laser molecular beam epitaxy using HVPE grown GaN bulk target. AIP Adv. **3**, 092109 (2013)
21. M. Senthil Kumar, S.S. Kushvaha, K.K. Maurya, K. Saravanan, S. Ojha, High resolution X-ray diffraction and Rutherford backscattering spectroscopy studies on laser molecular beam epitaxy grown GaN layers on sapphire (0001). Adv. Sci. Lett. **20**, 1406 (2014)
22. S.S. Kushvaha, M. Senthil Kumar, M. Maheshwari, A.K. Shukla, P. Pal, K.K. Maurya, Structural and electronic properties of epitaxial GaN layer grown on sapphire (0001) using laser molecular beam epitaxy. Mater. Res. Express **1**, 035903 (2014)
23. M. Senthil Kumar, K.M.K. Srivatsa, S.S. Kushvaha, Detection of dislocation-related midgap levels in pulsed laser deposited GaN by photo-induced current transient spectroscopy. Phys. Stat. Sol. (b) **252**, 800 (2015)
24. S.S. Kushvaha, M. Senthil Kumar, B.S. Yadav, P.K. Tyagi, S. Ojha, K.K. Maurya, B.P. Singh, Influence of laser repetition rate on the structural and optical properties of GaN layers grown on sapphire (0001) by laser molecular beam epitaxy. Cryst. Eng. Comm. **18**, 744 (2016)
25. Z. Zhong, F. Qian, D. Wang, C.M. Lieber, Synthesis of p-type gallium nitride nanowires for electronic and photonic nanodevices. Nano Lett. **3**, 343 (2003)
26. Y. Huang, X. Duan, Y. Cui, C.M. Lieber, Gallium nitride nanowire nanodevices. Nano Lett. **2**, 101 (2002)
27. A.T.M.G. Sarwar, S.D. Carnevale, F. Yang, T.F. Kent, J.J. Jamison, D.W. McComb, R.C. Myers, Semiconductor nanowire light-emitting diodes grown on metal: a direction toward large-scale fabrication of nanowire devices. Small **11**, 5402 (2015)
28. Z. Mi, S. Zhao, S.Y. Woo, M. Bugnet, M. Djavid, X. Liu, J. Kang, X. Kong, W. Ji, H. Guo, Z. Liu, G.A. Botton, Molecular beam epitaxial growth and characterization of Al(Ga)N nanowire deep ultraviolet light emitting diodes and lasers. J. Phys. D Appl. Phys. **49**, 364006 (2016)
29. R. Calarco, M. Marso, T. Richter, A.I. Aykanat, R. Meijers, A.V.T. Hart, T. Stoica, H. Lüth, Size-dependent photoconductivity in MBE-grown GaN-nanowires. Nano Lett. **5**, 981 (2008)
30. H.P. Bhasker, V. Thakur, S.M. Shivaprasad, S. Dhar, Quantum coherence of electrons in random networks of c-axis oriented wedge-shaped GaN nanowalls grown by molecular beam epitaxy. J. Phys. D Appl. Phys. **48**, 255302 (2015)
31. H.P. Bhasker, V. Thakur, M. Kesaria, S.M. Shivaprasad, S. Dhar, Transport and optical properties of c-axis oriented wedge shaped GaN nanowall network grown by molecular beam epitaxy. AIP Conf. Proc. **1583**, 252 (2014)

32. C.-H. Lee, Y.-J. Kim, J. Lee, Y.J. Hong, J.-M. Jeon, M. Kim, S. Hong, G.-C. Yi, Scalable network electrical devices using ZnO nanowalls. Nanotechnology **22**, 055205 (2011)
33. B.Q. Cao, T. Matsumoto, M. Matsumoto, M. Higashihata, D. Nakamura, T. Okada, ZnO nanowalls grown with high-pressure PLD and their applications as field emitters and UV detectors. J. Phys. Chem. C **113**, 10975 (2009)
34. A. Zhong, K. Hane, Growth of GaN nanowall network on Si (111) substrate by molecular beam epitaxy. Nanoscale Res. Lett. **7**, 686 (2012)
35. D. Poppitz, A. Lotnyk, J.W. Gerlach, B. Rauschenbach, Microstructure of porous gallium nitride nanowall networks. Acta Mater. **65**, 98 (2014)
36. S.S. Kushvaha, M. Senthil Kumar, A.K. Shukla, B.S. Yadav, D.K. Singh, M. Jewariya, S.R. Ragam, K.K. Maurya, Structural, optical and electronic properties of homoepitaxial GaN nanowalls grown on GaN template by laser molecular beam epitaxy. RSC Adv. **5**, 87818 (2015)
37. E.J. Tarsa, B. Heying, X.H. Wu, P. Fini, S.P. DenBaars, J.S. Speck, Homoepitaxial growth of GaN under Ga-stable and N-stable conditions by plasma-assisted molecular beam epitaxy. J. Appl. Phys. **82**, 5472 (1997)
38. B. Heying, R. Averbeck, L.F. Chen, E. Haus, H. Riechert, J.S. Speck, Control of GaN surface morphologies using plasma-assisted molecular beam epitaxy. J. Appl. Phys. **88**, 1855 (2000)
39. M. Kesaria, S. Shetty, S.M. Shivaprasad, Evidence for dislocation induced spontaneous formation of GaN nanowalls and nanocolumns on bare C-plane sapphire. Cryst. Growth Des. **11**, 4900 (2011)
40. A. Zhong, K. Hane, Characterization of GaN nanowall network and optical property of InGaN/GaN quantum wells by molecular beam epitaxy. Jpn. J. Appl. Phys. **52**, 08JE13 (2013)
41. V. Thakur, M. Kesaria, S.M. Shivaprasad, Enhanced band edge luminescence from stress and defect free GaN nanowall network morphology. Solid State Comm. **171**, 8 (2013)
42. M. Kesaria, S.M. Shivaprasad, Nitrogen flux induced GaN nanostructure nucleation at misfit dislocations on Al_2O_3 (0001). Appl. Phys. Lett. **99**, 143105 (2011)
43. K.A. Bertness, A. Roshko, L.M. Mansfield, T.E. Harvey, N.A. Sanford, Mechanism for spontaneous growth of GaN nanowires with molecular beam epitaxy. J. Cryst. Growth **310**, 3154 (2008)
44. Z.C. Feng, W. Wang, S.J. Chua, P.X. Zhang, K.P.J. Williams, G.D. Pitt, Raman scattering properties of GaN thin films grown on sapphire under visible and ultraviolet excitation. J. Raman Spectrosc. **32**, 840 (2001)
45. A. Kasic, D. Gogova, H. Larsson, C. Hemmingsson, I. Ivanov, B. Monemar, C. Bundesmann, M. Schubert, Micro-Raman scattering profiling studies on HVPE-grown free-standing GaN. Phys. Stat. Sol. (a) **201**, 2773 (2004)
46. V.Y. Davydov, Y.E. Kitaev, I.N. Goncharuk, A.N. Smirnov, J. Graul, O. Semchinova, D. Uffman, M.B. Smirnov, A.P. Mirgorodsky, R.A. Evarestov, Phonon dispersion and Raman scattering in hexagonal GaN and AlN. Phys. Rev. B **58**, 12899 (1998)
47. M.A. Reshchikov, H. Morkoc, Luminescence properties of defects in GaN. J. Appl. Phys. **97**, 061301 (2005)
48. M. Kesaria, S. Shetty, S.M. Shivaprasad, Spontaneous formation of GaN nanostructures by molecular beam epitaxy. J. Cryst. Growth **326**, 191 (2011)
49. H.P. Bhasker, S. Dhar, A. Sain, M. Kesaria, S.M. Shivaprasad, High electron mobility through the edge states in random networks of c-axis oriented wedge-shaped GaN nanowalls grown by molecular beam epitaxy. Appl. Phys. Lett. **101**, 132109 (2012)
50. C.C. Wu, D.S. Wuu, T.N. Chen, T.E. Yu, P.R. Lin, R.H. Horng, H.Y. Lai, Growth and characterization of epitaxial ZnO Nanowall networks using metal organic chemical vapor deposition. Jpn. J. Appl. Phys. **47**, 746 (2008)
51. B. Ha, S.H. Seo, J.H. Cho, C.S. Yoon, J. Yoo, G.C. Yi, C.Y. Park, C.J. Lee, Optical and field emission properties of thin single-crystalline GaN nanowires. J. Phys. Chem. B **109**, 11095 (2005)
52. M.R. Coan, J.H. Woo, D. Johnson, I.R. Gatabi, H.R. Harris, Band offset measurements of the GaN/dielectric interfaces. J. Appl. Phys. **112**, 024508 (2012)

53. D. Li, M. Sumiya, S. Fuke, D. Yang, D. Que, Y. Suzuki, Y. Fukuda, Selective etching of GaN polar surface in potassium hydroxide solution studied by X-ray photoelectron spectroscopy. J. Appl. Phys. **90**, 4219 (2001)
54. S.D. Wolter, B.P. Luther, D.L. Waltemyer, C. Önneby, S.E. Mohney, R.J. Molnar, X-ray photoelectron spectroscopy and X-ray diffraction study of the thermal oxide on gallium nitride. Appl. Phys. Lett. **70**, 2156 (1997)
55. M. Petravic, V.A. Coleman, K.J. Kim, B. Kim, G. Li, Defect acceptor and donor in ion-bombarded GaN. J. Vac. Sci. Technol. A **23**, 1340 (2005)
56. Y.-J. Lin, C.-D. Tsai, Y.-T. Lyu, C.-T. Lee, X-ray photoelectron spectroscopy study of (NH4) 2Sx-treated Mg-doped GaN layers. Appl. Phys. Lett. **77**, 687 (2000)
57. J.J. Yeh, I. Lindau, Atomic subshell photoionization cross sections and asymmetry parameters: $1 \leq Z \leq 103$. At. Data Nucl. Data Tables **32**, 1 (1985)
58. S. Tanuma, C.J. Powell, D.R. Penn, Calculations of electron inelastic mean free paths. V. data for 14 organic compounds over the 50–2000 eV range. Surf. Interface Anal. **21**, 165 (1993)
59. G. Koblmüller, J. Brown, R. Averbeck, H. Riechert, P. Pongratz, J.S. Speck, Continuous evolution of Ga adlayer coverages during plasma-assisted molecular-beam epitaxy of (0001) GaN. Appl. Phys. Lett. **86**, 041908 (2005)
60. S.H. Xu, H. Wu, X.Q. Dai, W.P. Lau, L.X. Zheng, M.H. Xie, S.Y. Tong, Direct observation of a Ga adlayer on a GaN (0001) surface by LEED Patterson inversion. Phys. Rev. B **67**, 125409 (2003)
61. A.R. Smith, R.M. Feenstra, D.W. Greve, J. Neugebauer, J.E. Northrup, Reconstructions of the GaN(000-1) Surface. Phys. Rev. Lett. **79**, 3934 (1997)
62. W. Lei, D. Liu, J. Zhang, B. Liu, P. Zhu, T. Cui, Q. Cui, G. Zou, AlN nanostructures: tunable architectures and optical properties. Chem. Comm. 1365 (2009)
63. K.A. Rickert, A.B. Ellis, F.J. Himpsel, J. Sun, T.F. Kuech, N–GaN surface treatments for metal contacts studied via X-ray photoemission spectroscopy. Appl. Phys. Lett. **80**, 204 (2002)
64. H.W. Jang, J.L. Lee, Origin of the abnormal behavior of contact resistance in ohmic contacts to laser-irradiated n-type GaN. Appl. Phys. Lett. **94**, 182108 (2009)
65. T. Hashizume, R. Nakasaki, Discrete surface state related to nitrogen-vacancy defect on plasma-treated GaN surfaces. Appl. Phys. Lett. **80**, 4564 (2002)
66. Y.J. Lin, Y.L. Chu, Effect of reactive ion etching-induced defects on the surface band bending of heavily Mg-doped p-type GaN. J. Appl. Phys. **97**, 104904 (2005)
67. M.G. Ganchenkova, R.M. Nieminen, Nitrogen vacancies as major point defects in gallium nitride. Phys. Rev. Lett. **96**, 196402 (2006)
68. D.J. Carter, M. Fuchs, C. Stampfl, Vacancies in GaN bulk and nanowires: effect of self-interaction corrections. J. Phys. Condens. Matter **24**, 255801 (2012)
69. F. Gao, E.J. Bylaska, A. El-Azab, W.J. Webber, Wannier orbitals and bonding properties of interstitial and antisite defects in GaN. Appl. Phys. Lett. **85**, 5565 (2004)
70. W.R.L. Lambrecht, B. Segall, S. Strite, G. Martin, A. Agarwal, H. Morkoc, A. Rockett, X-ray photoelectron spectroscopy and theory of the valence band and semicore Ga 3d states in GaN. Phys. Rev. B **50**, 14155 (1994)
71. P. Lorenz, T. Haensel, R. Gutt, R.J. Koch, J.A. Schaefer, S. Krischok, Analysis of polar GaN surfaces with photoelectron and high resolution electron energy loss spectroscopy. Phys. Stat. Sol. (b) **247**, 1658 (2010)
72. D. Skuridina, D.V. Dinh, B. Lacroix, P. Ruterana, M. Hoffmann, Z. Sitar, M. Pristovsek, M. Kneissl, P. Vogt, Polarity determination of polar and semipolar (11-22) InN and GaN layers by valence band photoemission spectroscopy. J. Appl. Phys. **114**, 173503 (2013)
73. M.A. Garcia, S.D. Wolter, T.-H. Kim, S. Choi, J. Baier, A. Brown, M. Losurdo, G. Bruno, Surface oxide relationships to band bending in GaN. Appl. Phys. Lett. **88**, 013506 (2006)
74. S.S. Kushvaha, M. Senthil Kumar, *Advances in Nanomaterials* (Springer, India, 2016)
75. S. Siddhanta, V. Thakur, C. Narayana, S.M. Shivaprasad, Universal metal-semiconductor hybrid nanostructured SERS substrate for biosensing. ACS Appl. Mater. Interfaces. **4**, 5807 (2012)